physica status solidi (RRL) – Rapid Research Letters

RESEARCH ARTICLE OPEN ACCESS

Circular Photocurrents in Large-Area Polycrystalline Tellurium Thin Films

Eleonora Bonaventura[1,2] | Chiara Massetti[2] | Matteo Gardella[2] | Sara Ghomi[2] | Carlo Grazianetti[2] | Christian Martella[2] | Alessandro Molle[2] | Jacopo Pedrini[1] | Fabio Pezzoli[1] | Emiliano Bonera[1]

[1]Dipartimento di Scienza dei Materiali, BiQuTe, Università degli Studi di Milano-Bicocca, Milan, Italy | [2]CNR-IMM, Agrate Brianza Unit, Agrate Brianza, Italy

Correspondence: Eleonora Bonaventura (eleonora.bonaventura@unimib.it) | Emiliano Bonera (emiliano.bonera@unimib.it)

Received: 19 September 2025 | **Revised:** 30 January 2026 | **Accepted:** 16 February 2026

Keywords: chirality | circular photogalvanic effect | photocurrent | tellurium

ABSTRACT

Helicity-sensitive photocurrents provide a direct fingerprint of broken inversion symmetry and spin–orbit coupling in quantum materials. However, it is unclear whether they persist in structurally disordered systems. Here, we report the observation of the circular photocurrents in polycrystalline tellurium (Te) thin films grown via physical vapor deposition. Under zero-bias illumination with circularly polarized light, the photocurrent exhibits the well-defined modulation characteristic of circular photogalvanic effect (CPGE). While the traditional fitting procedure makes assumptions about the structure of the signal, we also use a Fourier-based approach to extract the full set of periodic components in a model-independent way. This reveals a dominant term linked to reflectivity modulation and a distinct contribution consistent with a helicity-sensitive response. The emergence of the CPGE in a film composed of randomly oriented Te nanocrystals is attributed to its intrinsic circular dichroism. These results demonstrate that chirality-driven photocurrents can persist in disordered systems lacking long-range crystalline order. Spin- and polarization-dependent effects are thus compatible with scalable, polycrystalline architectures, supporting their integration into chiral optoelectronic and spintronic platforms.

1 | Introduction

In systems lacking inversion symmetry and exhibiting strong spin–orbit coupling, effects such as the circular photogalvanic effect (CPGE) and circular photon drag effect (CPDE) provide insight into spin textures and nontrivial band topology [1, 2]. These phenomena have emerged as powerful tools for unveiling hidden electronic structures and identifying topological features beyond the reach of conventional transport measurements [3–6]. CPGE was originally observed in semiconductor quantum wells [7] and later extensively reviewed as a general manifestation of spin photocurrents in gyrotropic systems [8]. In addition to their fundamental significance, light-induced currents enable rectified, polarization-sensitive photoresponses, paving the way for next-generation photonic and spintronic devices.

Among the materials exhibiting strong nonlinear and spin–orbit-driven optical phenomena, elemental tellurium (Te) has been extensively investigated. Te is a group VI semiconducting chalcogen with a noncentrosymmetric trigonal crystal structure, where atoms arrange into helical chains along the c-axis. These chains form a hexagonal array via weaker van der Waals interactions, resulting in a lattice composed of a central helix surrounded by six neighbors [9]. Its chiral structure, pronounced anisotropy, and the emergence of Weyl nodes near the conduction band edge make Te an ideal platform to explore the interplay between symmetry, nonlinear optics, and spin-polarized transport. However, current growth technologies do not permit the large-scale implementations of fully monocrystalline Te films.

Despite extensive work on CPGE and related effects in high-quality tellurium single crystals or flakes [10–15], little is known about the persistence and robustness of these phenomena

in polycrystalline Te films, where grain boundaries and structural disorder may strongly influence spin-dependent transport. Addressing this question is crucial for assessing the viability of scalable, low-cost optoelectronic devices. In this work, we investigate polarization-dependent photocurrents in Te thin films grown by physical vapor deposition (PVD). Our results demonstrate that helicity-sensitive photocurrents persist in the presence of polycrystallinity, revealing that chirality-driven signals can emerge even in structurally disordered systems.

2 | Results and Discussion

Te films were deposited on SiO_2/Si substrates using the PVD method with a nominal thickness of 65 nm uniformly covering an area of approximately 1 cm^2 [16]. The AFM morphology image measured on 1 μm × 1 μm area of a typical Te film considered in this experiment is reported in Figure 1a. The topography shows the formation of continuous Te grains with a roughness of tens of nanometers. The SEM images of Te nanostructures are presented in Figure 1b confirming the distribution of grains on a relatively large scale. A Raman spectrum of the Te films is reported in Figure 1c, showing two main peaks at 123.5 and 141.6 cm^{-1}. These peaks can be assigned to the out-of-plane (A_1) and in-plane (E_2) Raman active modes of the Te lattice. Lorentzian fitting yields full width at half maximum (FWHM) values of 7.8 and 8.5 cm^{-1}, respectively, higher than those of bulk Te and so consistent with the polycrystalline nature of the films [17].

To measure the photocurrent response, Te thin films were integrated into device architecture with a standard Hall bar geometry (Figure 1d-e). This geometry has already proven effective in several previous works on CPGE in tellurium and related systems [14, 15, 18]. Following channel definition and deposition of the metallic contacts, a conformal Al_2O_3 capping layer was deposited via atomic layer deposition to protect the structure. A subsequent lithographic step provided access to the contact pads. Photocurrent measurements were performed using contacts A and B, as indicated in Figure 1e, positioned along the *x*-direction of the Hall bar. Electrical characterization of these two contacts, shown in Figure 1f, confirmed ohmic behavior, with a resistivity at room temperature of ~3 Ω·cm. This value, which is found to be strongly affected by the thickness of the film and the size of the grains, is consistent with those reported in the literature for polycrystalline Te films [19, 20].

The experimental setup for photocurrent measurements is illustrated in Figure 2a–b. The sample is illuminated with a continuous-wave laser under ambient conditions, and the spontaneous photocurrent (i.e., measured under zero bias) is recorded. To isolate the CPGE from other polarization-dependent contributions, the incident light polarization is modulated using a quarterwave plate (QWP). The beam impinges on the sample at an incident angle $\alpha_1 = 30°$. While the QWP is rotated continuously the polarization changes from linear to circular, i.e. right-handed (RCP) and left-handed (LCP) circular polarizations. During this modulation, both the reflected light intensity and the photocurrent are recorded simultaneously. The latter is amplified via a transimpedance amplifier and measured with a lock-in amplifier synchronized to the frequency of an optical chopper placed in the beam path.

As the QWP angle varies, the photocurrent signal evolves periodically and can be described as a sum of cosine components of the form $I_p \cos[p\,(\theta - \Phi_p)]$ where p denotes the periodicity, I_p the amplitude, and Φ_p the phase of each harmonic contribution. In systems exhibiting CPGE, the dominant contributions are typically [3, 8]

$$I = I_2 \cos[2(\theta - \Phi_2)] + I_4 \cos[4(\theta - \Phi_4)] + I_0 \quad (1)$$

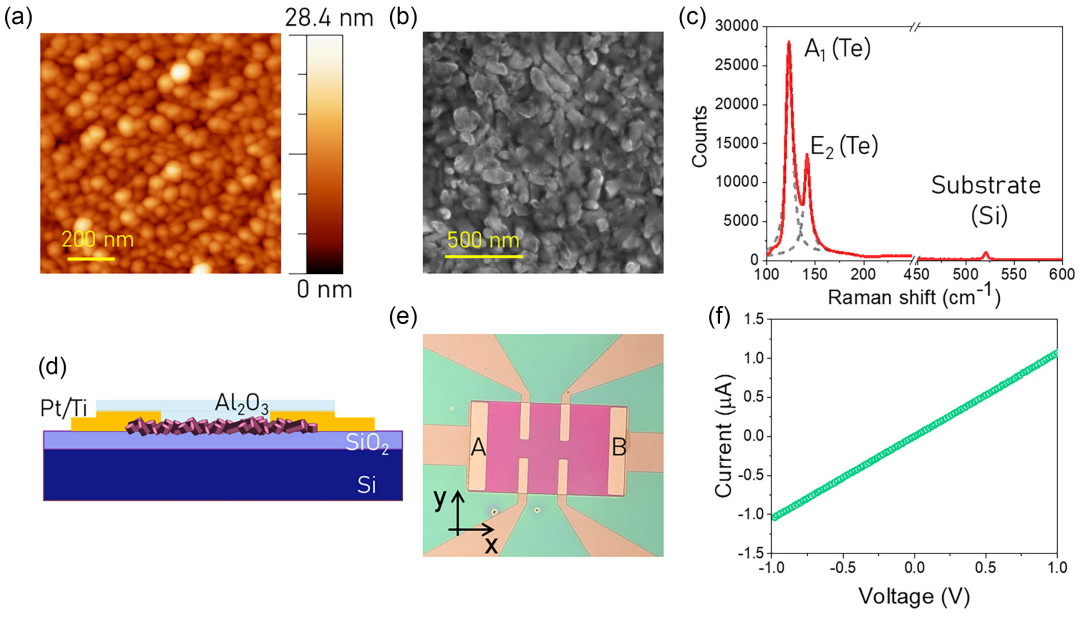

FIGURE 1 | (a,b) AFM and SEM morphological analysis of the Te films grown on SiO_2/Si substrates. (c) Typical Raman spectrum of the Te nanostructures on SiO_2/Si substrate. (d) Schematic of the device architecture. (e) Optical microscope image of the device. Contacts A and B are used for photocurrent measurements. (f) *I–V* curve of the device measured along the *x*-axis, using A and B contacts.

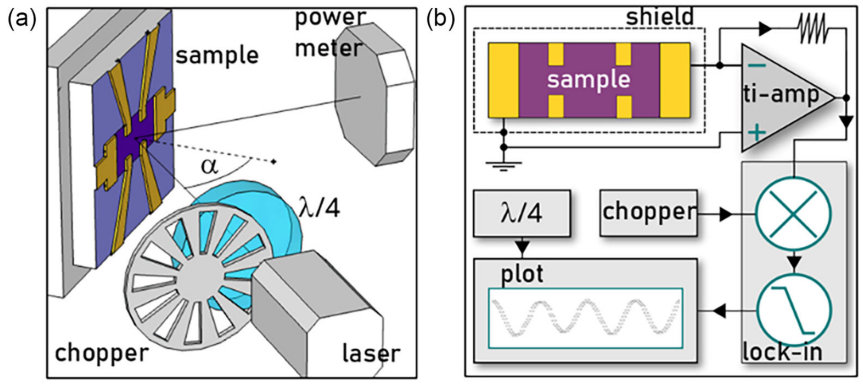

FIGURE 2 | (a) Geometry of the setup used for photocurrent measurements and (b) electrical scheme.

where the $p=2$ component arises from the helicity-sensitive CPGE (period π), the $p=4$ term originates from reflectivity modulations described by Fresnel equations, and I_0 ($p=0$) parameterizes polarization-independent contributions.

The reflectivity and photocurrent signals are shown in Figure 3a,b. The measurements were performed by rotating the QWP over two full cycles ($\theta = 0 \rightarrow 4\pi$) to rule out drifts and enhance the accuracy of the Fourier analysis presented later. Figure 3a displays the reflectance of the sample (i.e. the measured signal is normalized to the incident laser power), where minima correspond to maximal absorption in Te. The modulation follows Fresnel's laws for light polarization evolving from pure s-polarization (LP) to a superposition of s- and p-components (RCP and LCP). It is well described by a sinusoidal term with periodicity $p=4$ and phase shift $\Phi_4 = \pi/2$.

The reflectivity measurement was synchronized with the photocurrent acquisition. The photocurrent signal (Figure 3b) shows clear periodic modulation that matches the periodicity of the reflectance. The dominant $p=4$ component closely follows the reflectivity trend, suggesting that it originates from periodic optical absorption variation rather than circular polarization. Therefore, it is independent of the helicity of the incident light. This component is commonly attributed to built-in photovoltaic effects [15], which are also responsible for the polarization-independent contribution ($p=0$). Specifically, surface n-type doping, which is induced by the Al_2O_3 capping layer, may form a p–n junction with the intrinsically p-doped Te bulk, leading to zero-bias charge separation under illumination. Additional contributions from thermoelectric effects due to inhomogeneous illumination may also play a role in this respect. Importantly, these contributions account for background photocurrent components and do not exhibit helicity dependence associated with circularly polarized excitation. Conversely, the formation of Schottky barriers at the contacts can be excluded based on prior confirmation of ohmic behavior. It is important to note that the photocurrent cannot be fully described by a single $p=4$ harmonic. A comparison with the reflectivity signal reveals an asymmetry between the odd and even minima, pointing to the presence of a $p=2$ component.

The data were fitted using Equation (1) . This analysis confirms the coexistence of three contributions, whose parameters are listed in Table 1. Under oblique light incidence, the extracted component may in principle arise from multiple mechanisms, including the CPGE and the CPDE [21, 22]. These two contributions originate from nonlinear optical processes of different order: CPGE is governed by a third-order tensor, whereas CPDE requires a fourth-order tensor contribution [14]. Since lower-order nonlinear

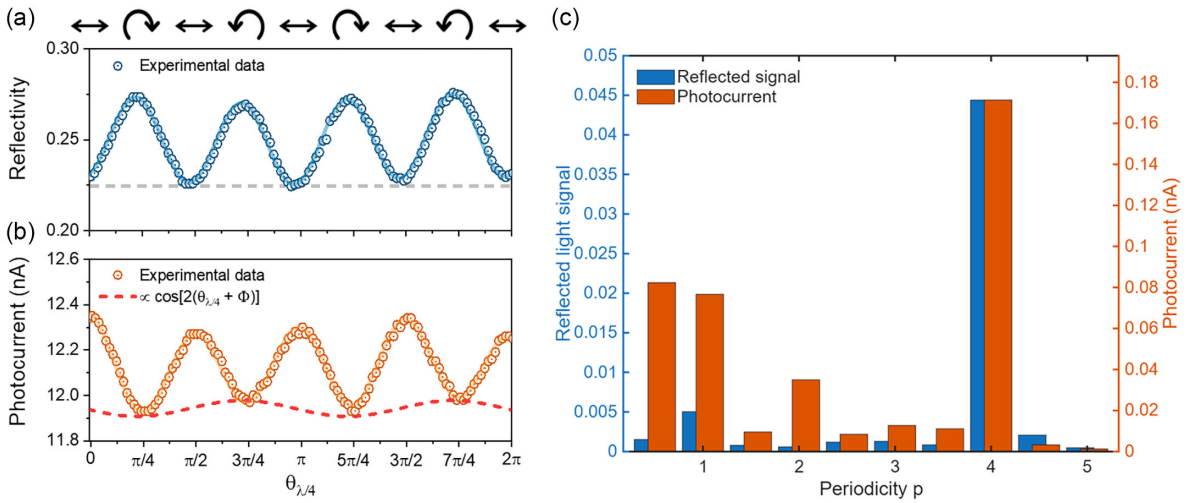

FIGURE 3 | $\theta_{\lambda/4}$-dependent signals under 1300 nm excitation on the Te device. (a) Reflectivity. (b) Photocurrent. (c) Reflected light signal and photocurrent Fourier components. The component with a periodicity of 2 is related to the CPGE. The 0-component was removed for clarity.

TABLE 1 | Comparison of the parameters obtained from the fitting procedure and from the Fourier analysis.

	Fourier		Fit	
p	***I* (nA)**	**F (rad)**	***I* (nA)**	**F (rad)**
0	12.167	—	12.13	—
1	0.0766	−0.09	—	—
2	0.0349	1.79	0.0197	1.73
4	0.1714	0.61	0.1701	0.605

processes typically produce stronger responses under comparable excitation conditions, the magnitude and periodicity of the observed helicity-sensitive signal support a dominant CPGE contribution, in agreement with previously reported CPGE signatures in tellurium flakes [14, 15]. It is important to stress that, unlike THz-based experiments probing intraband Weyl-cone dynamics, the present measurements are performed at higher photon energies, in the near-infrared spectral range, where CPGE is experimentally observed without direct access to the underlying microscopic relaxation pathways.

The use of Equation (1) imposes a constraint on the number and type of periodic components used to describe the photocurrent, typically limiting the analysis to the polarization-independent effects ($p=0$), the expected CPGE ($p=2$) and reflectivity-related ($p=4$) harmonics. However, this approach neglects the possible presence of additional terms arising from experimental rtefacts or complex material responses. To overcome this limitation, we apply a Fourier analysis to the measured signal, which enables a model-independent decomposition of the photocurrent into its harmonic contributions. Figure 3 c reports the normalized Fourier amplitudes of the reflectivity and photocurrent signals. The extended QWP rotation range ($\theta = 0 \rightarrow 4\pi$) ensures sufficient resolution to detect fractional periodicities down to 0.5 m, with m positive integer. Components at noninteger p values originate from low-frequency drifts or measurement noise and can thus be identified and filtered out. The explicit appearance of larger rtefact-related components in the Fourier spectrum represents the strength of the method, as it allows these contributions to be clearly identified and separated. The quantitative difference between the $p=2$ amplitudes obtained from Fourier analysis and analytical fitting (see Table 1) reflects the different assumptions underlying the two methods. While the analytical fit constrains the signal to a limited set of harmonics, the unconstrained Fourier decomposition allows all periodic components to emerge explicitly. As a result, the two approaches yield different amplitudes while consistently identifying the same $p=2$ contribution with comparable phase, confirming the robustness of the helicity-sensitive response.

In the reflectivity spectrum, the dominant harmonics are $p=0$, 1, and 4. The $p=1$ component arises from an rtefact in the illumination of the sample. Conversely, the photocurrent spectrum exhibits the $p=0$ component corresponding to a polarization-independent background current, a strong $p=4$ contribution consistent with the Fresnel-modulated absorption, and a distinct $p=2$ peak corresponding to the helicity-sensitive CPGE. Coherently, the amplitude of the $p=2$ component extracted from the Fourier analysis agrees well with that obtained via fitting to Equation (1) . As previously discussed, the observation of CPGE in a polycrystalline film composed of randomly oriented Te nanocrystals with opposite chirality suggests a net imbalance in the excitation between left- and right-handed domains. While the total absorption of photons is the same in both the left- and right-handed polarizations, the relative population of excited electrons in left- and right-handed domains is different in the two cases. This effect can be rationalized by the intrinsic circular dichroism of Te, arising from its low-symmetry, chiral crystal structure [23, 24]. If A_L and A_R denote the absorption coefficients of left- and right-handed enantiomers, the dissymmetry factor $g=2(A_L - A_R)/(A_L + A_R)$, quantifies the degree of chiral optical activity. Although specific values at 1300 nm are not available, typical g values in the near-infrared range are of the order of 10^{-2} [24], indicating that circularly polarized light can induce a measurable asymmetry in absorption. This also provides a useful framework within which to contextualize the magnitude of the helicity-sensitive photocurrent observed in polycrystalline films. CPGE amplitudes on the order of 10^{-5} A/W have been reported in high-quality tellurium flakes and single-crystal systems [14, 15], whereas the helicity-sensitive response in our polycrystalline films is on the order of 10^{-8} A/W. This reduction is consistent with the expected impact of structural disorder, grain boundaries, and random crystal orientation, which can suppress the net chiral response without eliminating it.

Notably, despite the reduced magnitude compared to single-crystal tellurium, the observation of a circular photocurrent in large-area polycrystalline tellurium films demonstrates the feasibility of implementing chiral optoelectronic functionalities in microelectronics-compatible platforms, with potential relevance for scalable polarization-sensitive applications.

3 | Conclusion

The application of Fourier analysis provides a powerful and unbiased method to decompose photocurrent signals into their harmonic components, without imposing a predefined functional form. This approach allows for the unambiguous identification of helicity-sensitive contributions such as CPGE or CPDE, even in complex systems where multiple effects coexist. The detection of a clear $p=2$ component in polycrystalline Te films confirms that chirality-driven photocurrent responses can persist despite structural disorder and random grain orientation. Previous works on tellurium single crystals showed that the responsivity of CPGE is orders of magnitude stronger than CPDE. This result highlights the robustness of the circular photocurrent mechanism in tellurium and reinforces the role of chiral optical absorption in enabling helicity-selective excitation at the nanoscale. More broadly, our findings suggest that, when properly engineered, polycrystalline chiral semiconductors can exhibit symmetry-sensitive nonlinear responses comparable to those of their single-crystal counterparts. Spin-selective and polarization-dependent effects are thus compatible with disordered chiral semiconductors, making them suitable for scalable applications. Future studies combining spatially resolved spectroscopy and

control over grain orientation may further elucidate the interplay between microstructure and macroscopic photocurrent generation in chiral systems.

4 | Experimental Methods

Synthesis: Te samples were grown in a dual zone vapor deposition reactor consisting of a 2″ quartz tube. 30 mg of Te powder were placed in an alumina boat located at the center of the upstream furnace and maintained at 440°C. A SiO_2/Si substrate was placed on a ceramic boat inside the downstream furnace at 16 cm far from the Te source. The downstream furnace was maintained at room temperature, and a flux of 10 sccm Ar/H_2 was employed as the carrier gas during the 30-min growth process. Further information is provided in Ref. [16].

Characterization: The morphology of the Te samples was examined using a Zeiss-SUPRA 40 field-emission SEM equipment in bright-field mode and a Bruker Dimension Edge atomic force microscope (AFM) equipped with ultrasharp silicon probes (nominal tip radius <10 nm) in the tapping mode. The crystalline quality of the films was also verified by micro-Raman spectroscopy. Spectra were collected using a Renishaw InVia spectrometer in backscattering configuration provided with a 50× objective with a 0.75 numerical aperture. A 514 nm solid-state laser was used for excitation, with a maximum power of 5 mW at the sample surface.

Fabrication: The Hall bar devices were patterned using the Tabletop Maskless Aligner μMLA (Heidelberg GmbH) to define the channel area and the electrical contacts. The active channels were isolated by etching the Te using a 1:10 diluted aqua regia solution (HNO_3 : HCl 1:3). 10/30 nm Ti/Pt metal contacts were deposited by DC magnetron sputtering followed by lift-off. After the Al_2O_3 deposition, a final lithography step was performed to etch square access areas into the alumina using a 1:50 diluted buffered oxide etchant (BOE) solution.

Circular polarized photocurrent measurements: A laser diode at 1300 nm was used to illuminate the samples. The collimated beam has a spot size of ˜1 mm and the incident power on the surface of the samples is 4.5 mW. A QWP appropriate for the corresponding wavelength and mounted on a motorized precision rotation stage driven by a servo monitor (Thorlabs) was used to control the polarization of the beam. The photocurrent was measured with a Zurich MFLI lock-in amplifier at room temperature. The incidence angle (set at 30° for this experiment) was controlled using a micrometer-controlled rotating stage.

Author Contributions

Eleonora Bonaventura: conceptualization (supporting), data curation (lead); formal analysis (lead); investigation (lead); methodology (equal); writing – original draft (lead); writing – review & editing (equal). **Chiara Massetti:** investigation (supporting), methodology (supporting), writing – review & editing (supporting). **Matteo Gardella:** investigation (supporting); writing – review & editing (supporting). **Sara Ghomi:** methodology (supporting), writing – review & editing (supporting). **Christian Martella:** writing – review & editing (supporting). **Carlo Grazianetti:** writing – review & editing (supporting). **Alessandro Molle:** funding acquisition (equal); writing – review & editing (supporting). **Jacopo Pedrini:** writing – review & editing (supporting). **Fabio Pezzoli:** conceptualization (supporting); funding acquisition (supporting), writing– review & editing (supporting). **Emiliano Bonera:** conceptualization (equal); funding acquisition (equal); investigation (supporting), methodology (supporting), supervision (lead); writing – original draft (supporting); writing – review & editing (supporting).

Acknowledgments

The authors would like to acknowledge L. M. Lombardi, M. Scarabelli, and N. Cavalleri for their technical assistance with the CPGE measurements and A. Cataldo for the alumina capping layer deposition. This publication was supported by the Ministero dell'Università e della Ricerca (MUR), call PRIN2020, project "PHOtonics Terahertz devices based on topological mate-rials" ("PHOTO"), grant no. 2020RPEPNH and PNRR MUR project PE0000023-NQST. F. P. acknowledges support by the Air Force Office of Scientific Research under the award number FA8655-22-1-7050.

Open access publishing facilitated by Universita degli Studi di Milano-Bicocca, as part of the Wiley - CRUI-CARE agreement.

Funding

This work was supported by Ministero dell'Università e della Ricerca (2020RPEPNH, PE0000023-NQST) and U.S. Air Force (FA8655-22-1-7050).

Conflicts of Interest

The authors declare no conflicts of interest.

Data Availability Statement

The data supporting the findings of this study are available from the corresponding author upon request.

References

1. C. K. Chan, N. H. Lindner, G. Refael, and P. A. Lee, "Photocurrents in Weyl Semimetals," *Physical Review. B* 95, no. 4 (2017): 041104.

2. G. Chang, B. J. Wieder, F. Schindler, et al., "Topological Quantum Properties of Chiral Crystals," *Nature Materials* 17, no. 11 (2018): 978–985.

3. J. W. McIver, D. Hsieh, H. Steinberg, P. Jarillo-Herrero, and N. Gedik, "Control over Topological Insulator Photocurrents with Light Polarization," *Nature Nanotechnology* 7, no. 2 (2012): 96–100.

4. H. Plank, L. E. Golub, S. Bauer, et al., "Photon Drag Effect in $(Bi_{1-x}Sb_x)_2Te_3$ Three-Dimensional Topological Insulators," *Physical Review. B* 93, no. 12 (2016): 125434.

5. Z. Ji, G. Liu, Z. Addison, et al., "Spatially Dispersive Circular Photogalvanic Effect in a Weyl Semimetal," *Nature Materials* 18, no. 9 (2019): 955–962.

6. Z. Ni, K. Wang, Y. Zhang, et al., "Giant Topological Longitudinal Circular Photo-Galvanic Effect in the Chiral Multifold Semimetal CoSi," *Nature Communications* 12, no. 1 (2021): 154.

7. S. D. Ganichev, E. L. Ivchenko, S. N. Danilov, et al., "Conversion of Spin into Directed Electric Current in Quantum Wells," *Physical Review Letters* 86, no. 19 (2001): 4358.

8. S. D. Ganichev and W. Prettl, "Spin Photocurrents in Quantum Wells," *Journal of Physics: Condensed Matter* 15, no. 20 (2003): R935.

9. E. J. Weidmann and J. C. Anderson, "Structure and Growth of Oriented Tellurium Thin Films," *Thin Solid Films* 7, no. 3-4 (1971): 265–276.

10. E. L. Ivchenko and G. E. Pikus, "New Photogalvanic Effect in Gyrotropic Crystals," *JETP Letters* 27 (1978): 604.

11. L. E. Vorob'ev, E. L. Ivchenko, G. E. Pikus, I. I. Farbshteĭn, V. A. Shalygin, and A. V. Shturbin, "Optical Activity in Tellurium Induced by a Current," *JETP Letters* 29 (1979): 441.

12. V. M. Asnin, A. A. Bakun, A. M. Danishevskii, E. L. Ivchenko, G. E. Pikus, and A. A. Rogachev, ""Circular" Photogalvanic Effect in Optically Active Crystals," *Solid State Communications* 30, no. 9 (1979): 565–570.

13. V. A. Shalygin, M. D. Moldavskaya, S. N. Danilov, I. I. Farbshtein, and L. E. Golub, "Circular Photon Drag Effect in Bulk Tellurium," *Physical Review. B* 93, no. 4 (2016): 045207.

14. J. Ma, B. Cheng, L. Li, et al., "Unveiling Weyl-Related Optical Responses in Semiconducting Tellurium by Mid-Infrared Circular Photogalvanic Effect," *Nature Communications* 13, no. 1 (2022): 5425.

15. C. Niu, S. Huang, N. Ghosh, et al., "Tunable Circular Photogalvanic and Photovoltaic Effect in 2D Tellurium with Different Chirality," *Nano Letters* 23, no. 8 (2023): 3599–3606.

16. S. Ghomi, P. P. Tummala, R. Cecchini, et al., "Tailoring the Dimensionality of Tellurium Nanostructures via Vapor Transport Growth," *Materials Science in Semiconductor Processing* 168 (2023): 107838.

17. A. S. Pine and G. Dresselhaus, "Raman Spectra and Lattice Dynamics of Tellurium," *Physical Review B* 4, no. 2 (1971): 356.

18. H. Yuan, X. Wang, B. Lian, et al., "Generation and Electric Control of Spin–valley-Coupled Circular Photogalvanic Current in WSe_2," *Nature Nanotechnology* 9, no. 10 (2014): 851–857.

19. G. Fischer, G. K. White, and S. B. Woods, "Thermal and Electrical Resistivity of Tellurium at Low Temperatures," *Physical Review* 106, no. 3 (1957): 480.

20. R. W. Dutton and R. S. Muller, "Electrical Properties of Tellurium Thin Films," *Proceedings of the IEEE* 59, no. 10 (1971): 1511–1517.

21. J. Quereda, T. S. Ghiasi, J.-S. You, J. van den Brink, B. J. van Wees, and C. H. van der Wal, "Symmetry Regimes for Circular Photocurrents in Monolayer $MoSe_2$," *Nature Communications* 9, no. 1 (2018): 3346.

22. Y. Zhao, F. Chen, J. Liang, et al., "Origin of Nonlinear Circular Photocurrent in 2D Semiconductor MoS_2," *Physical Review Letters* 134, no. 8 (2025): 086201.

23. A. Londoño-Calderon, D. J. Williams, M. M. Schneider, et al., "Intrinsic Helical Twist and Chirality in Ultrathin Tellurium Nanowires," *Nanoscale* 13, no. 21 (2021): 9606–9614.

24. B. Reuven, A. Movsesyan, E. Y. Santiago, et al., "Anisotropic Circular Dichroism in Aligned Chiral Tellurium Nanorods," *Advanced Optical Materials* 11, no. 18 (2023): 2203142.